STATIC BENDING RESPONSE OF VARIABLE THICKNESS FGM PLATES USING NEW SHEAR DEFORMATION PLATE THEORY

Thi Cam Nhung Nguyen[1], Thi Huong Huyen Truong[1,*]

[1]*Faculty of Mechanical Engineering, Le Quy Don Technical University*

Abstract

This study aims to investigate the static bending behavior of functionally graded material plates with variable thickness using a new shear deformation theory and the finite element method. Material and mechanical models are developed to establish the equations describing mechanical relationships. The calculation program is implemented in MATLAB, and its accuracy is verified by comparison with results from analytical methods presented in reputable scientific publications. The error between methods is no more than 1.5%. The program can calculate plate structures with variable thickness according to different rules such as linear and nonlinear. The effects of geometric and material parameters on the static bending of FGM plates with variable thickness are explored. Following this, the thickness change affects the bending of the plate. These results provide an essential foundation for addressing more complex problems in the future.

Keywords: *Variable thickness; FGM; static bending; new shear deformation plate theory; FEM.*

1. Introduction

Plate structures are widely utilized in engineering applications and have long been a focal point for scientific investigation, especially when exploring new calculation methods or theoretical approaches. With the rapid advancements in material science, cutting-edge materials are being developed and employed across industries such as defense, aerospace, and automotive engineering. This article analyzes the static bending response of functionally graded material (FGM) plates with varying thicknesses, utilizing a novel shear deformation theory alongside the finite element method (FEM). Before delving into the core analysis, a concise review of related studies is provided.

Most recently, A. Mamandi [1] used the first-order shear deformation theory (FSDT) to conduct a FEM-based bending analysis of rectangular FGM plates with variable boundary conditions and transverse stresses. Three distinct FGM models are under consideration: P-FGM, S-FGM, and E-FGM. S. S. Yadav *et al*. [2] demonstrated the bending evaluation of FGM plates using sinusoidal shear and normal deformation theory. To account for the effect of transverse shear deformation, in-plane displacements

[*] Corresponding author, email: huonghuyen.hvktqs@gmail.com
DOI: 10.56651/lqdtu.jst.v20.n02.902

used sinusoidal functions in the thickness coordinate, whereas transverse displacements used the cosine function in the thickness coordinate. N. T. H. Van *et al*. [3] investigated the static bending and natural oscillation properties of double-layer, non-uniform thickness functionally graded (FG) plates with shear connections. The fundamental equations were thoroughly defined and constructed using the FEM in combination with the widely accepted and simple FSDT. S. R. Li *et al.* [4] proposed classical and homogenized formulas for the bending solutions of FGM plates based on the four variable plate theories. V. N. V. Hoang and P. T. Thanh [5] introduced a novel trigonometric shear deformation plate theory (TSDPT) for free vibration analysis of FG plates with two-directional variable thicknesses. L. Hadji *et al*. [6] developed a displacement-based high-order shear deformation theory to explain the static response of functionally graded plates. It did not need the shear correction factor. It caused transverse shear stress fluctuation, which varied parabolically over the thickness to meet free surface requirements for shear stress. V. T. Do *et al*. [7] used one unknown variable in the displacement formula and an analytical approach based on the Navier solution to give information about the development of refined plate theory to study the static bending behavior of FGM plates.

A thorough review of existing literature reveals a considerable gap in studying the static bending behavior of FGM plates. While various shear deformation theories have been used to analyze FGM plates, no previous research has specifically investigated the bending response of variable-thickness FGM plates using the new shear deformation theory combined with the FEM. This article presents a novel shear deformation method that enhances accuracy across a wide range of structural thicknesses, from thick to ultra-thin, without requiring shear correction factors. Compared to traditional models such as FSDT and TSDPT, this approach yields more precise solutions. However, its primary drawback lies in the increased computational complexity. This study aims to fill that gap by introducing a novel theoretical framework and computational approach, offering improved accuracy in predicting stress distribution and deformation characteristics.

2. Finite element formulation

2.1. Fundamental equations

Consider a variable thickness FG plate as shown in Fig. 1. The geometrical dimensions are length *a*, width *b*, and variable thickness of the plate *h* (*x*, *y*).

The plate is made of FG material with a volume proportion of ceramic (V_c) and metal (V_m) described by a simple power-law distribution [8]:

$$\begin{cases} V_c = \left(\dfrac{1}{2} + \dfrac{z}{h(x,y)}\right)^n & \text{with} \quad -0.5h(x,y) \le z \le 0.5h(x,y) \\ V_m = 1 - V_c \end{cases} \tag{1}$$

The variable *n* denotes the index of volume fraction. The variable *z* indicates the coordinate of thickness. The subscripts "*m*" and "*c*" reflect the metal and ceramic elements, respectively.

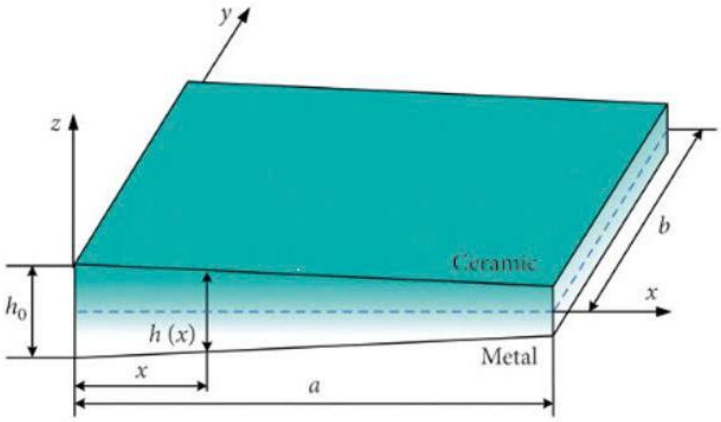

Fig. 1. FGM plate model with variable thickness.

The elastic modulus (*E*) and Poisson's ratio (ν), in this research, are calculated as [8]:

$$P(z) = P_m + (P_c - P_m)\, V_c \tag{2}$$

where *P* is the mechanical characteristics of the material.

Based on the new shear deformation theory, the displacement field at any point in the plate is calculated as:

$$\begin{cases} u = u_o - z\dfrac{\partial w_0}{\partial x} + f(z)\varphi_x \\ v = v_o - z\dfrac{\partial w_0}{\partial y} + f(z)\varphi_y \\ w = w_o \end{cases} \tag{3}$$

where u_0, v_0, w_0 are the displacements in the horizontal and vertical planes, respectively, φ_x, φ_y are the angular quantities of rotation about the axes Ox, Oy. Let $\beta_x = \dfrac{\partial w_0}{\partial x}$ and $\beta_y = \dfrac{\partial w_0}{\partial y}$, the displacement field is rewritten as follows [9]:

$$\begin{cases} u = u_o - z\beta_x + f(z)\varphi_x \\ v = v_o - z\beta_y + f(z)\varphi_y \\ w = w_o \end{cases}$$

The bending strain is calculated as follows:

$$\bar{\varepsilon} = \begin{Bmatrix} \dfrac{\partial u}{\partial x} \\ \dfrac{\partial v}{\partial y} \\ \dfrac{\partial u}{\partial y} + \dfrac{\partial v}{\partial x} \end{Bmatrix} = \begin{Bmatrix} \dfrac{\partial u_o}{\partial x} - z\dfrac{\partial \beta_x}{\partial x} + f(z)\dfrac{\partial \varphi_x}{\partial x} \\ \dfrac{\partial v_o}{\partial y} - z\dfrac{\partial \beta_y}{\partial y} + f(z)\dfrac{\partial \varphi_y}{\partial y} \\ \dfrac{\partial u_o}{\partial y} + \dfrac{\partial v_o}{\partial x} - z\left(\dfrac{\partial \beta_x}{\partial y} + \dfrac{\partial \beta_y}{\partial x}\right) + f(z)\left(\dfrac{\partial \varphi_x}{\partial y} + \dfrac{\partial \varphi_y}{\partial x}\right) \end{Bmatrix}$$

Let us divide the strain components as follows:

$$\varepsilon_1 = \begin{Bmatrix} \dfrac{\partial u_o}{\partial x} \\ \dfrac{\partial v_o}{\partial y} \\ \dfrac{\partial u_o}{\partial y} + \dfrac{\partial v_o}{\partial x} \end{Bmatrix}; \varepsilon_2 = \begin{Bmatrix} \dfrac{\partial \beta_x}{\partial x} \\ \dfrac{\partial \beta_y}{\partial y} \\ \dfrac{\partial \beta_x}{\partial y} + \dfrac{\partial \beta_y}{\partial x} \end{Bmatrix}; \varepsilon_3 = \begin{Bmatrix} \dfrac{\partial \varphi_x}{\partial x} \\ \dfrac{\partial \varphi_y}{\partial y} \\ \dfrac{\partial \varphi_x}{\partial y} + \dfrac{\partial \varphi_y}{\partial x} \end{Bmatrix}$$

Then, we have the bending deformation component in reduced form:

$$\bar{\varepsilon} = \varepsilon_1 + z\varepsilon_2 + f(z)\varepsilon_3 \tag{4}$$

The shear strain component is calculated as follows:

$$\gamma = \begin{Bmatrix} \gamma_{xz} \\ \gamma_{yz} \end{Bmatrix} = \begin{Bmatrix} \dfrac{\partial u}{\partial z} + \dfrac{\partial w}{\partial x} \\ \dfrac{\partial v}{\partial z} + \dfrac{\partial w}{\partial y} \end{Bmatrix} = \begin{Bmatrix} \beta_x - \dfrac{\partial w_0}{\partial x} + f'(z)\varphi_x \\ \beta_y - \dfrac{\partial w_0}{\partial y} + f'(z)\varphi_y \end{Bmatrix} = \varepsilon_{s1} + f'(z)\varepsilon_{s2}$$

where

$$\varepsilon_{s1} = \begin{Bmatrix} \beta_x - \dfrac{\partial w_0}{\partial x} \\ \beta_y - \dfrac{\partial w_0}{\partial y} \end{Bmatrix}; \varepsilon_{s2} = \begin{Bmatrix} \varphi_x \\ \varphi_y \end{Bmatrix}$$

The stress field is calculated through the strain field and material properties based on Hooke's law as follows:

$$\begin{Bmatrix} \sigma_{xx} \\ \sigma_{yy} \\ \tau_{xy} \\ \tau_{xz} \\ \tau_{yz} \end{Bmatrix} = \begin{bmatrix} C_{11} & C_{12} & 0 & 0 & 0 \\ C_{21} & C_{22} & 0 & 0 & 0 \\ 0 & 0 & C_{66} & 0 & 0 \\ 0 & 0 & 0 & C_{55} & 0 \\ 0 & 0 & 0 & 0 & C_{44} \end{bmatrix} \begin{Bmatrix} \varepsilon_{xx} \\ \varepsilon_{yy} \\ \gamma_{xy} \\ \gamma_{xz} \\ \gamma_{yz} \end{Bmatrix}$$

where $C_{11} = C_{22} = \dfrac{E_e}{1-\nu_e^2}$, $C_{12} = \dfrac{\nu_e E_e}{1-\nu_e^2}$, $C_{66} = C_{55} = C_{44} = \dfrac{E_e}{2(1+\nu_e)}$.

The elastic strain potential energy is calculated as follows:

$$U = \frac{1}{2}\int_{V_e} \{\varepsilon\}^T \{\sigma\} dV_e = \frac{1}{2}\int_{S_e} \left(\delta\bar{\varepsilon} C^b \bar{\varepsilon} + \delta\gamma C^s \gamma\right) dxdy \tag{5}$$

where $\bar{\boldsymbol{\varepsilon}} = \begin{Bmatrix} \boldsymbol{\varepsilon}_1 \\ \boldsymbol{\varepsilon}_2 \\ \boldsymbol{\varepsilon}_3 \end{Bmatrix}$, $\bar{\boldsymbol{\gamma}} = \begin{Bmatrix} \boldsymbol{\varepsilon}_{s1} \\ \boldsymbol{\varepsilon}_{s2} \end{Bmatrix}$, $\mathbf{C}^b = \begin{bmatrix} \mathbf{A} & \mathbf{B} & \mathbf{E} \\ \mathbf{B} & \mathbf{D} & \mathbf{F} \\ \mathbf{E} & \mathbf{F} & \mathbf{H} \end{bmatrix}$, $\mathbf{C}^s = \begin{bmatrix} \mathbf{A}^s & \mathbf{B}^s \\ \mathbf{B}^s & \mathbf{D}^s \end{bmatrix}$,

$$\left(A_{ij}, B_{ij}, D_{ij}, E_{ij}, F_{ij}, H_{ij}\right) = \int_{-h/2}^{h/2} \left(1, z, z^2, f(z), zf(z), f^2(z)\right) C_{ij} dz$$

where $(i, j = 1, 2, 6)$.

$$\left(A_{ij}^s, B_{ij}^s, D_{ij}^s\right) = \int_{-h/2}^{h/2} \left(1, f'(z), f'^2(z)\right) C_{ij} dz$$

where $(i, j = 4, 5)$.

This study employs a four-node quadrilateral element, each node having seven degrees of freedom. The approximation is based on the Lagrange function Q4 (N_i) as:

$$\underset{28x1}{\{q_e\}} = \begin{Bmatrix} \{q_1\} \\ \{q_2\} \\ \{q_3\} \\ \{q_4\} \end{Bmatrix}; \underset{7x1}{\{q_i\}} = \begin{Bmatrix} u_{0i} \\ v_{0i} \\ w_{0i} \\ \beta_{xi} \\ \beta_{yi} \\ \varphi_{xi} \\ \varphi_{yi} \end{Bmatrix} \quad \underset{28x1}{\{q_e\}} = \begin{Bmatrix} \{q_1\} \\ \{q_2\} \\ \{q_3\} \\ \{q_4\} \end{Bmatrix}; \underset{7x1}{\{q_i\}} = \begin{Bmatrix} u_{0i} \\ v_{0i} \\ w_{0i} \\ \beta_{xi} \\ \beta_{yi} \\ \varphi_{xi} \\ \varphi_{yi} \end{Bmatrix}$$

The displacement components are now calculated as follows:

$$u_0 = \sum_{i=1}^{4} u_{oi} N_i = H^u q_e; v_0 = \sum_{i=1}^{4} v_{oi} N_i = H^v q_e; w_0 = \sum_{i=1}^{4} w_{oi} N_i = H^w q_e;$$

$$\beta_x = \sum_{i=1}^{4} \beta_{xi} H_i = H^{\beta x} q_e; \beta_y = \sum_{i=1}^{4} \beta_{yi} H_i = H^{\beta y} q_e; \varphi_x = \sum_{i=1}^{4} \varphi_{xi} N_i = H^{\varphi x} q_e$$

$$\varphi_y = \sum_{i=1}^{4} \varphi_{yi} N_i = H^{\varphi y} q_e$$

where $N^u, N^v, N^w, H^{\beta x}, H^{\beta y}, H^{\varphi x},$ and $H^{\varphi y}$ are calculated as follows:

$$H^u = \left[N_1 \;\; zeros(1,6) \;\; N_2 \;\; zeros(1,6) \;\; N_3 \;\; zeros(1,6) \;\; N_4 \;\; zeros(1,6)\right];$$
$$H^v = \left[zeros(1,1) \;\; N_1 \;\; zeros(1,6) \;\; N_2 \;\; zeros(1,6) \;\; N_3 \;\; zeros(1,6) \;\; N_4 \;\; zeros(1,5)\right];$$
$$H^w = \left[zeros(1,2) \;\; N_1 \;\; zeros(1,6) \;\; N_2 \;\; zeros(1,6) \;\; N_3 \;\; zeros(1,6) \;\; N_4 \;\; zeros(1,4)\right];$$
$$H^{\beta x} = \left[zeros(1,3) \;\; N_1 \;\; zeros(1,6) \;\; N_2 \;\; zeros(1,6) \;\; N_3 \;\; zeros(1,6) \;\; N_4 \;\; zeros(1,3)\right];$$
$$H^{\beta y} = \left[zeros(1,4) \;\; N_1 \;\; zeros(1,6) \;\; N_2 \;\; zeros(1,6) \;\; N_3 \;\; zeros(1,6) \;\; N_4 \;\; zeros(1,2)\right];$$
$$H^{\varphi x} = \left[zeros(1,5) \;\; N_1 \;\; zeros(1,6) \;\; N_2 \;\; zeros(1,6) \;\; N_3 \;\; zeros(1,6) \;\; N_4 \;\; zeros(1,1)\right];$$
$$H^{\varphi y} = \left[zeros(1,6) \;\; N_1 \;\; zeros(1,6) \;\; N_2 \;\; zeros(1,6) \;\; N_3 \;\; zeros(1,6) \;\; N_4\right];$$

The strain components are then calculated through the differential matrices of the shape functions and the displacement vectors of the elements:

$$\varepsilon_1 = \mathbf{B}_1 q_e; \varepsilon_2 = \mathbf{B}_2 q_e; \varepsilon_3 = \mathbf{B}_3 q_e; \varepsilon_{s1} = \mathbf{B}_{s1} q_e; \varepsilon_{s2} = \mathbf{B}_{s2} q_e;$$

where

$$\mathbf{B}_1 = \begin{bmatrix} H^u_{,x} \\ H^v_{,y} \\ H^u_{,y} + H^v_{,x} \end{bmatrix}; \mathbf{B}_2 = \begin{bmatrix} H^{\beta x}_{,x} \\ H^{\beta y}_{,y} \\ H^{\beta x}_{,y} + H^{\beta y}_{,x} \end{bmatrix}; \mathbf{B}_3 = \begin{bmatrix} H^{\varphi x}_{,x} \\ H^{\varphi y}_{,y} \\ H^{\varphi x}_{,y} + H^{\varphi y}_{,x} \end{bmatrix};$$

$$\mathbf{B}_{1s} = \begin{bmatrix} -H^w_{,x} + H^{\beta x} \\ -H^w_{,y} + H^{\beta y} \end{bmatrix}; \mathbf{B}_{2s} = \begin{bmatrix} H^{\varphi x} \\ H^{\varphi y} \end{bmatrix}$$

The stiffness matrix is now calculated as follows:

$$\boldsymbol{K}_e = \int_{lx} \int_{ly} \left(B^T C^b B + B_s^T C^s B_s \right) dxdy \tag{6}$$

Herein, **T** denotes the transition matrix and

$$\mathbf{B}=\begin{bmatrix}\mathbf{B}_1\\ \mathbf{B}_2\\ \mathbf{B}_2\end{bmatrix};\mathbf{B}_s=\begin{bmatrix}\mathbf{B}_{s1}\\ \mathbf{B}_{s2}\end{bmatrix}$$

Let us examine an external distribution load $q(x,y)$ applied to the plate's upper surface. By employing the law of virtual work, therefore, the energy performed by an external load can be expressed as:

$$W_e=\int_{S_e}\{w\}^T\ \boldsymbol{p}dS_e \tag{7}$$

in which $\boldsymbol{p}$ is the vector of nodal load that is determined as:

$$\boldsymbol{p}=\begin{Bmatrix}0 & 0 & 0 & 0 & q(x,y) & 0 & 0 & 0 & 0\end{Bmatrix}^T \tag{8}$$

The result of substituting Eq. (8) for Eq. (7) is:

$$W_e=\boldsymbol{q}_e^T\left(\int_{S_e}\left[H^w\right]^T\ \boldsymbol{p}dxdy\right)=\boldsymbol{q}_e^T.\boldsymbol{F}_e \tag{9}$$

Consequently, the vector of element nodal force is acquired as:

$$\underset{28x1}{\{F_e\}}=\int_{S_e}\underset{28x1}{\left[H^w\right]^T}\ \boldsymbol{p}dxdy \tag{10}$$

The global matrix of stiffness $\mathbf{K}$ and the global vector of force $\boldsymbol{F}$ are generated by combining the element matrix of stiffness $\mathbf{K}_e$ and the element vector of force $\boldsymbol{F}_e$.

The equation utilized for the static issue is as:

$$\mathbf{F}=\mathbf{K}.\boldsymbol{Q} \tag{11}$$

where $\boldsymbol{Q}$ is the vector of global displacements.

2.2. Boundary conditions

When an element node has a simple support: $u_0=w_0=\beta_x=\varphi_x$ at x = 0, a and $v_0=w_0=\beta_y=\varphi_y$ at y = 0, b.

When an element node has a clamped support: $u_0=w_0=\beta_x=\varphi_x=v_0=\beta_y=\varphi_y$ at all edges.

Therefore, some types of boundary conditions used in this article are as follows: CCCC, SSSS, CSCS, CCSS, CFFF, and CFCF (where *C* denotes a clamped edge, *S* is a simply supported edge, and *F* is a free edge).

3. Numerical results and discussions

MATLAB software is employed to develop algorithms for calculating the static bending of FGM plates with varying thicknesses using the existing equations and the finite element approach. The precision of this program set is validated through numerical comparison with credible publications, thus examining and discussing the impact of input parameters on the plate's static bending capacity.

3.1. Accuracy of the calculation program

Consider an isotropic plate with a thickness that varies and material properties $E = 2 \cdot 10^9$ Pa, $\nu = 0.3$, as illustrated in Fig. 2 and [10]. The plate is subjected to a short-edge clamping connection, resulting from a uniformly distributed force on the plate surface with an intensity of p = 2000 (N/m^2). The error is calculated by the formula $\varepsilon = \frac{|[10] - present|}{[10]} \cdot 100\%$ with data taken from [10] and this work. In Tab. 1, the displacements at specific locations of the plate are compared to [10]. It is evident that the results proposed in the article and the published results are identical, with an error of no more than 1.5%. This illustrates the accuracy of the model and methodology established in the article.

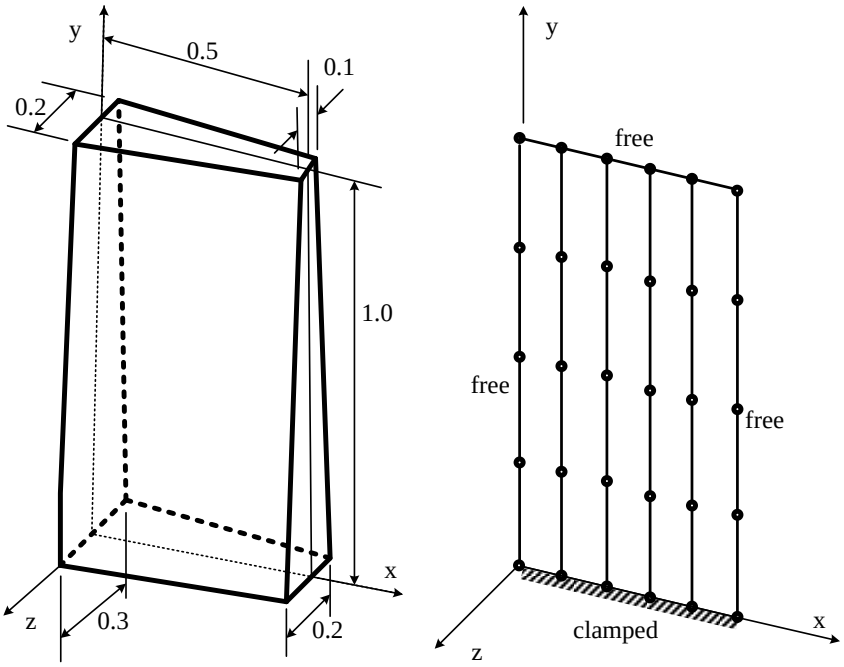

Fig. 2. FGM plate model with variable thickness [10].

Tab. 1. Deflection (μm) at some points of the plate with varying thickness

Along the *y*-axis at $x = 0.25$				**Along the *x*-axis at** $y = 1$			
Coordinate (y)	This work	[10]	Error (%)	Coordinate (x)	This work	[10]	Error (%)
0.000	0.000	0.000	0	0.000	1.144	1.140	0.35
0.125	0.049	0.050	1.04	0.0625	1.159	1.155	0.35
0.250	0.139	0.137	1.44	0.125	1.173	1.171	0.17
0.038	0.266	0.269	1.13	0.1875	1.188	1.185	0.25
0.500	0.423	0.426	0.71	0.250	1.203	1.200	0.25
0.625	0.603	0.601	0.33	0.313	1.218	1.213	0.41
0.750	0.798	0.800	0.25	0.375	1.232	1.230	0.16
0.875	1.000	0.990	1.00	0.438	1.246	1.243	0.24
1.000	1.203	1.200	0.25	0.500	1.259	1.260	0.08

3.2. Parameter study

Tab. 2. Convergence of dimensionless vertical displacements of square isotropic plates concerning the number of plate elements

Boundary conditions	Number of meshes					[11]
	8 × 8	10 × 10	12 × 12	16 × 16	20 × 20	
SSSS	4.2455	4.2630	4.2660	4.2690	4.2704	4.2702
CCCC	1.4865	1.4983	1.5002	1.5022	1.5030	1.5026

First, the convergence of the dimensionless vertical displacement results at the center point of the isotropic square plate concerning the number of plate elements is verified. The input parameters and the vertical displacement results at the center point of the plate can be found in [11]. The results show that, with the number of 16 × 16 elements, the displacement values converge with high accuracy for both considered boundary conditions. Therefore, the number of 16 × 16 meshes will be used for all subsequent studies.

This subsection examines and discusses the impact of various geometrical and

material factors of the plate on its displacement response. The parameters of the plate are specified as follows: FGM plate exhibiting variable thickness (Fig. 1) with dimensions $a = b = 1$ m; $h_0 = 0.3$ m; $h_1 = h_2 = 0.2$ m. In this article, four types of boundary conditions are taken into calculation. The substance comprises two elements: The ceramic material (Al_2O_3) possesses an elastic modulus E_c of $380 \cdot 10^9$ Pa and a Poisson's ratio v_c of 0.3. The metal material (Al) has an elastic modulus E_m of $70 \cdot 10^9$ Pa, a Poisson's ratio v_m of 0.3, and a volume fraction exponent n of 1. The plate is subjected to an evenly distributed load of $p = 1000$ Pa perpendicular to its plane.

Figure 3 and Table 2 illustrate that the FGM plate, with a uniform thickness, is subjected to a four-sided simple support configuration. Upon application of an evenly distributed force on the plate surface, the displacement field exhibits a symmetrical configuration with the highest displacement occurring in the center of the plate (Fig. 3a). However, when the plate thickness varies uniformly along the x and y axes, the displacement field is altered. The displacement center relocates toward the plate with reduced thickness (Fig. 3b). The maximum displacement of the plate with a linearly varying thickness along the x and y axes is less than that of the plate with a uniform thickness ($h = 0.3$ m).

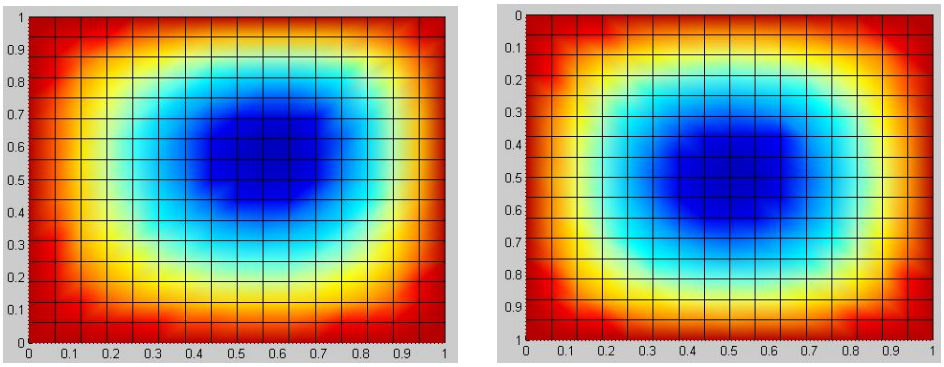

(a) *(b)*

Fig. 3. The displacement field of the plate

a) Plate with variable thickness; b) Plate with constant thickness.

Tab. 2. Dimensionless maximum displacement

Dimensionless maximum displacement	**Plate with variable thickness**	**Plate with constant thickness**
$w_1 = \dfrac{10wh^3Ec}{Pa^4}$	3.49	1.12

3.3. Effect of thickness change rule

Let us consider an FGM with geometrical and material properties as presented in Section 3.2. The plate is under an SSSS boundary condition. The plate has a thickness variation in the *x* and *y* directions.

Consider four cases:

- Case 1: Thickness varies linearly along one edge:

$$h_0 = h_2 = 0.1;\ h_1 = 0.2;\ h = h(x) = h_0\left(1 + x\frac{h_1 - h_0}{a}\right) \text{ (m)}.$$

- Case 2: Thickness varies linearly along the *x*- and *y*-axes:

$$h_0 = 0.1;\ h_1 = h_2 = 0.2;\ h = h_0 h(x) h(y);\ \begin{cases} h(x) = \left(1 + x\dfrac{h_1 - h_0}{a}\right) \\ h(y) = \left(1 + y\dfrac{h_2 - h_0}{b}\right) \end{cases} \text{ (m)}.$$

- Case 3: Quadratic thickness variation along one edge:

$$h_0 = 0.1;\quad h(x) = h_0\left(1 - \frac{x^2}{10}\right) \text{ (m)}.$$

- Case 4: Quadratic thickness variation along 2 edges:

$$h_0 = 0.1;\quad h(x) = h_0\left(1 - \frac{x^2}{5}\right)\left(1 - \frac{y^2}{5}\right) \text{ (m)}.$$

The displacement field of the plate is shown in Fig. 4. The maximum dimensionless displacement is shown in Table 3. From Fig. 4, we can see that, in the case where the thickness changes in one direction (*x* direction) (case 1, case 3), the displacement center moves in the *x* direction, deviating towards the side with the smaller thickness, the *y* direction does not change. In case 2, the thickness changes in both the *x* and *y* directions, so the displacement center is deviated towards the side with the smaller thickness. In case 4, the plate has a constant thickness, and the displacement center is at the center of the plate. With the boundary condition: clamping one edge, the deflection of the plate along the *y*-axis at $x = 0.5$ and the *x*-axis with $y = 1$ changes, but for the plate with a constant thickness, the displacement at all points along the *x*-axis at $y = 1$ remains constant. This proves that the thickness change affects the bending of the plate.

Tab. 3. Dimensionless maximum displacement

Dimensionless maximum displacement	**Case 1**	**Case 2**	**Case 3**	**Case 4**
$w_1 = \frac{10wh^3Ec}{Pa^4}$	0.72	0.63	1.12	1.25

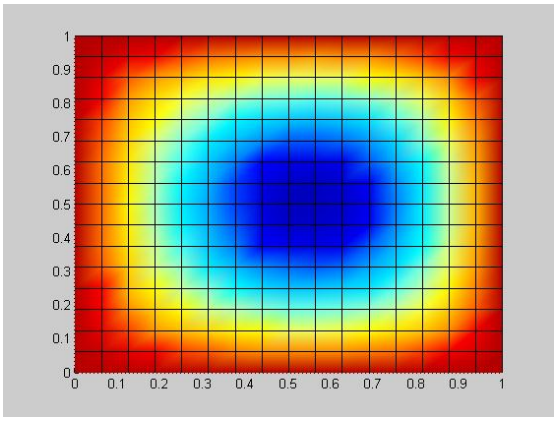

(a) Case 1

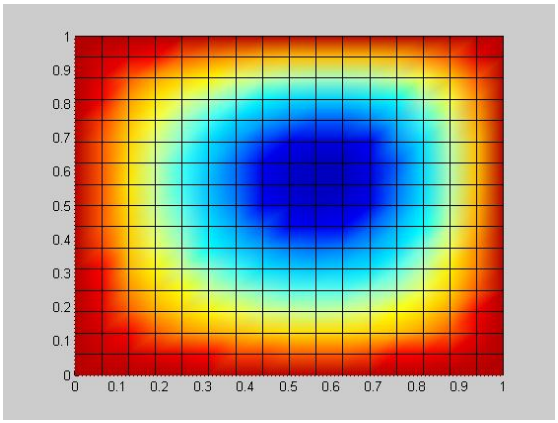

(b) Case 2

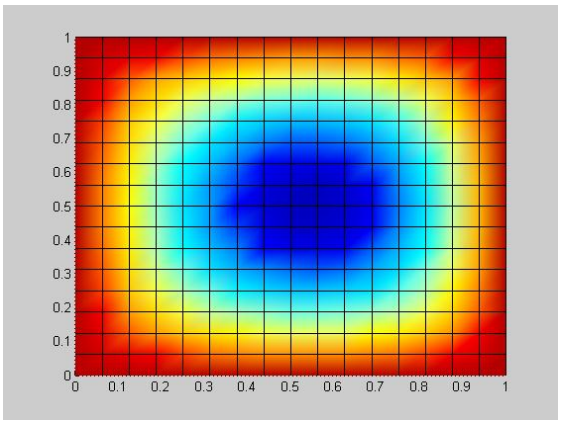

(c) Case 3

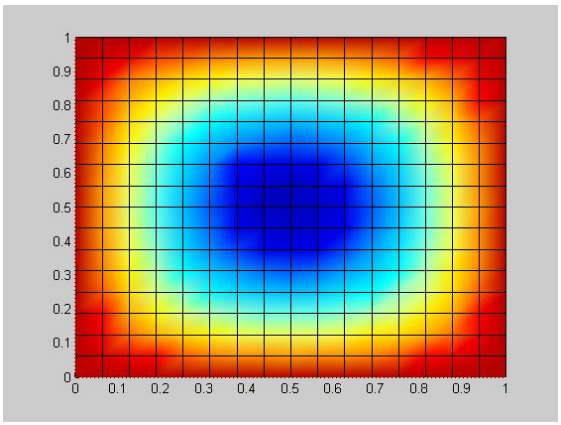

(d) Case 4

Fig. 4. The displacement field of FGM plate with variable thickness.

3.4. Influence of material volume exponential coefficient

Figure 5 illustrates the effect of the material volume exponential coefficient on the midpoint displacement of the plate $w_1 = \frac{10wh^3Ec}{Pa^4}$. The exponent n ranges from 0 to 10. The results indicate that as n transitions from 0 to 2, the displacement value

increases the fastest, due to the strong shift from the harsher ceramic material to the softer metal material; From 2 to 10, the displacement value $w_1 = \dfrac{10wh^3Ec}{Pa^4}$ rises more slowly, because the metal component has now become significant. The observed rise in n results in a decrease in structural rigidity, attributed to the heightened metal concentration at this juncture. Figure 5 shows that under the CCCC boundary condition, a stiffer structure reduces displacement. Conversely, under the SSSS boundary condition, the structure is more flexible, leading to a greater displacement. The displacement difference at n = 0 for case (c) is approximately 1.7 times. Similarly, for cases (a), (b), and (d), the difference ranges from 1.7 to 1.8 times. Moreover, it is evident that varying boundary conditions substantially influence the displacement value of the plate.

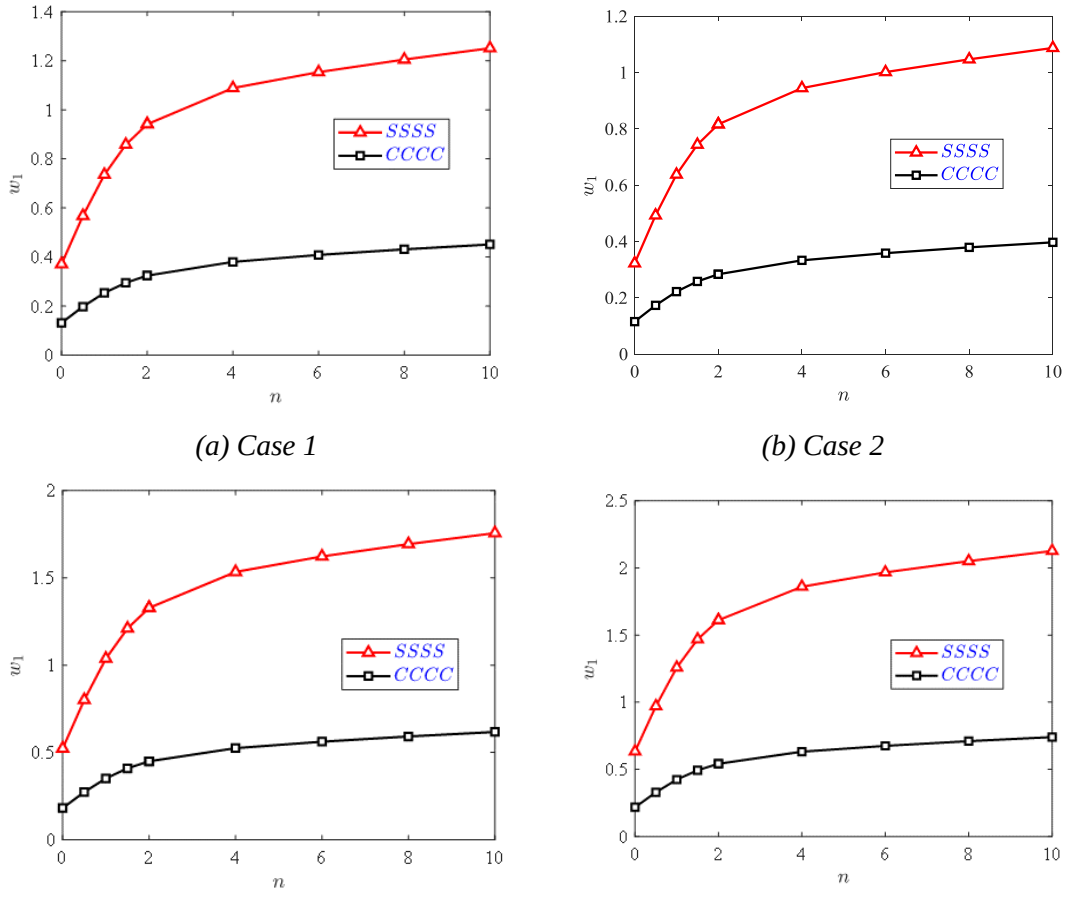

(a) Case 1 *(b) Case 2*

(c) Case 3 *(d) Case 4*

Fig. 5. Change of displacement response due to change of material exponential coefficient.

4. Conclusion

This article presents a finite element method based on high-order shear deformation theory for static bending analysis of FGM plates with variable thickness. A quadrilateral element with 4 nodes, each node with 7 degrees of freedom, is approximated based on the Lagrange Q4 function to establish the stiffness matrix components and force vector of the element. The program is capable of calculating plate structures with variable thickness according to different rules such as linear and nonlinear. The accuracy of the method has been verified through numerical comparison with reliable publications. A set of bending results calculated due to the influence of geometric parameters and plate materials is discovered. These results can be used as reference documents for researchers, designing structures with variable thickness in practice. Future studies such as natural vibration problems, stability, and dynamics of structures with variable thickness may benefit from the results of this study.

Acknowledgment

This research is funded by the Le Quy Don Technical University Research Fund under the grant number 24.1.21.

References

[1] A. Mamandi, "Finite element based bending analysis of rectangular FGM plates using first-order shear deformation theory", *Journal of Mechanical Science and Technology*, Vol. 37, No. 5, pp. 2491-2506, 2023. DOI: 10.1007/s12206-023-0425-6

[2] S. S. Yadav *et al.*, "Bending analysis of FGM plates using sinusoidal shear and normal deformation theory", *Forces in Mechanics*, Vol. 11, 2023. DOI: 10.1016/j.finmec.2023.100185

[3] N. T. H. Van *et al.*, "Finite-element modeling for static bending and free vibration analyses of double-layer non-uniform thickness FG plates taking into account sliding interactions", *Archives of Civil and Mechanical Engineering*, Vol. 24, No. 2, 2024. DOI: 10.1007/s43452-024-00914-9

[4] S. R. Li *et al.*, "Classical and homogenized expressions for the bending solutions of FGM plates based on the four variable plate theories", *Mechanics of Advanced Materials and Structures*, Vol. 31, No. 15, pp. 3413-3424, 2024. DOI: 10.1080/15376494.2023.2177909

[5] V. N. V. Hoang and P. T. Thanh, "A new trigonometric shear deformation plate theory for free vibration analysis of FGM plates with two-directional variable thickness", *Thin-Walled Structures*, Vol. 194, 2024. DOI: 10.1016/j.tws.2023.111310

[6] L. Hadji *et al.*, "Investigation of the static bending response of FGM sandwich plates", *Journal of Applied and Computational Mechanics*, Vol. 10, No. 1, pp. 26-37, 2024. DOI: 10.22055/jacm.2023.44278.4194

[7] V. T. Do *et al.*, "On the development of refined plate theory for static bending behavior of functionally graded plates", *Mathematical Problems in Engineering*, Vol. 2020, 2020. DOI: 10.1155/2020/2836763

[8] L. M. Thai *et al.*, "Finite-element modeling for static bending analysis of rotating two-layer FGM beams with shear connectors resting on imperfect elastic foundations", *Journal of Aerospace Engineering*, Vol. 36, No. 3, 2023. DOI: 10.1061/jaeeez.aseng-4771

[9] C. H. Thai *et al.*, "A nonlocal strain gradient isogeometric model for free vibration and bending analyses of functionally graded plates", *Composite Structures*, Vol. 251, 2020. DOI: 10.1016/j.compstruct.2020.112634

[10] P. Gagnon *et al.*, "A finite strip element for the analysis of variable thickness rectangular thick plates", *Computers & Structures*, Vol. 63, No. 2, pp. 349-362, 1997. DOI: 10.1016/S0045-7949(96)00018-1

[11] J. N. Reddy, *Mechanics of Laminated Composite Plates and Shells: Theory and Analysis*. CRC Press, 2003.

PHÂN TÍCH UỐN TĨNH CỦA TẤM FGM CÓ ĐỘ DÀY BIẾN ĐỔI SỬ DỤNG LÝ THUYẾT BIẾN DẠNG CẮT KIỂU MỚI

Nguyễn Thị Cẩm Nhung[1], Trương Thị Hương Huyền[1]

[1]*Khoa Cơ khí, Trường Đại học Kỹ thuật Lê Quý Đôn*

Tóm tắt: Bài báo sử dụng lý thuyết biến dạng cắt kiểu mới và phương pháp phần tử hữu hạn để nghiên cứu uốn tĩnh của tấm FGM có độ dày thay đổi. Mô hình vật liệu và cơ học được thiết lập để xây dựng các phương trình quan hệ về cơ học. Chương trình tính toán được lập trình trong môi trường MATLAB và được xác minh tính chính xác thông qua so sánh với các kết quả từ phương pháp giải tích ở các công trình khoa học uy tín. Sai số giữa các phương pháp không quá 1,5%. Sau đó, ảnh hưởng của các thông số hình học và vật liệu đến uốn tĩnh của tấm FGM có chiều dày thay đổi được khảo sát. Chương trình có khả năng tính toán các tấm với độ dày thay đổi theo các quy tắc tuyến tính và phi tuyến. Tác động của các thông số hình học và vật liệu lên uốn tĩnh của tấm FGM có độ dày thay đổi cũng được khám phá, giúp làm rõ cách thay đổi độ dày ảnh hưởng đến độ uốn của tấm. Các kết quả tính toán là cơ sở quan trọng cho việc phát triển các bài toán phức tạp hơn trong tương lai.

Từ khóa: *Độ dày thay đổi; FGM; uốn tĩnh; lý thuyết biến dạng cắt kiểu mới; FEM.*

Received: 28/10/2024; Revised: 27/03/2025; Accepted for publication: 23/05/2025

❑